Hole Transport in a Chiral Nematic Phase

160°C

Circularly Polarized Light Emission

RCPL

RCPL

LCPL

LCPL
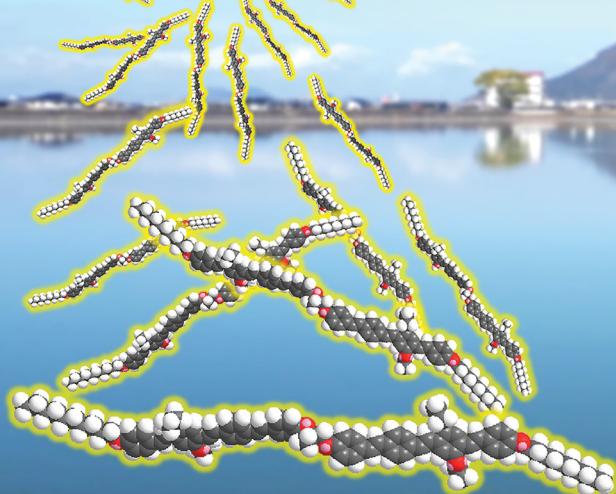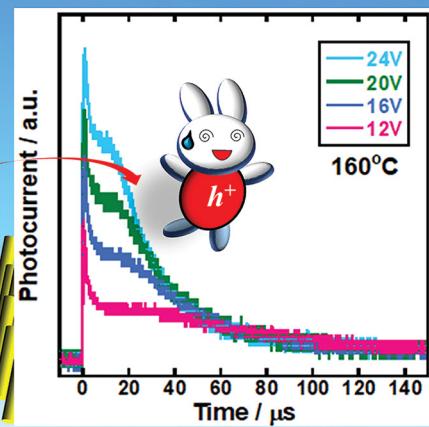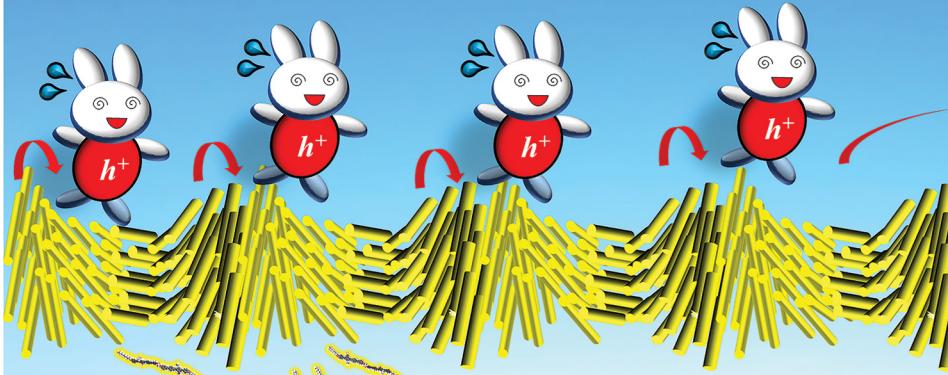
Chiral Dimer based on Oligo-PPV Units
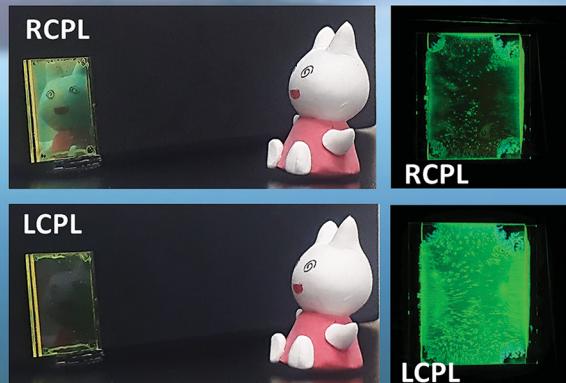
Carrier transport characteristics of glass-forming chiral liquid crystalline dimers based on oligo(phenylenevinylene) units

We synthesized dimeric chiral nematic (N*) liquid crystals bearing tri(*p*-phenylene vinylene) units, aiming at construction of an electrically pumped system for circularly polarized light emission. The mixture of the chiral liquid crystals exhibited a glassy N* phase at room temperature. The rod-like chromophore with the large aspect ratio enables the wide reflection band, resulting in the high quality circularly polarized light emission with the dissymmetry factor of 1.4. Hole mobilities were determined over wide temperature ranges by the TOF method and the hole transport characteristics were analysed by the Gaussian disorder model.

As featured in:
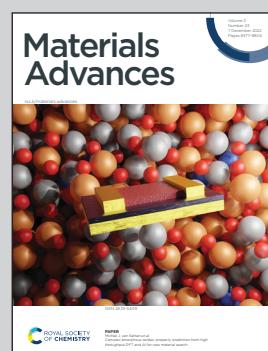
Materials Advances

ROYAL SOCIETY OF CHEMISTRY

rsc.li/materials-advances

Check for updates

Carrier transport characteristics of glass-forming chiral liquid crystalline dimers based on oligo(phenylenevinylene) units†

Masaki Kunihiro,‡[a] Eigo Shimaoka,§[a] Shuhei Morishita,[a] Noriaki Tsurumachi[a] and Masahiro Funahashi ✶[ab]

We synthesized chiral dimeric chiral nematic (N*) liquid crystals bearing tri(*p*-phenylene vinylene) units. The mixture of dimeric compounds and monomeric chiral liquid crystals exhibited a glassy N* phase at room temperature and the reflection band could be tuned by the change of the temperature from which the rapid cooling of the mixture started. When the reflection band covered the fluorescence peak, high quality circularly polarized emission with a dissymmetry factor of 1.4 was observed. Hole mobilities were determined over wide temperature ranges by the TOF method and the hole transport characteristics in the N* phase were analyzed using the Gaussian disorder model. The preexponential factors in the N* phase of these compounds, corresponding to a virtual mobility without energetic and spatial disorders, were one or two order of magnitudes higher than those of amorphous organic semiconductors. This should be attributed to the large π-conjugated units of these compounds. The energetic and spatial disorders were larger than those of amorphous organic semiconductors in spite of the local uniaxial molecular orientation in the N* phase. This result should be caused by the large anisotropic polarizability of the π-conjugated units with a large aspect ratio.

Introduction

Liquid crystals based on extended π-conjugated units exhibit electronic charge carrier transport.[1–4] This class of liquid crystals are known as liquid crystalline (LC) semiconductors and their application to polarized electroluminescence,[5–7] field-effect transistors,[8–12] and solar cells[13–15] has been studied extensively. In addition to solution-processability, flexibility, and good carrier transport properties, LC supramolecular structures constructed with nanosegregation or molecular chirality create new functions such as electrochromism,[16,17] the bulk photovoltaic effect,[18–20] and polarized electroluminescence.[21]

In a chiral nematic (N*) phase, helical supramolecular structures with periodicities of visible light wavelength are

formed, where circularly polarized light (CPL) emission and laser action have been observed.[22,23] For the construction of electrically pumped systems, N* liquid crystals comprising extended π-conjugated units with large aspect ratios have been studied.[24] High quality CPL emission within the wide reflection band over 200 nm and enhancement of fluorescence at the reflection band edge have been reported only in optically pumped systems.[25–28]

In order to realize electrically pumped systems, molecular design should be optimized for improvement of the carrier transport. Carrier transport properties in liquid crystal phases have been studied by means of a time-of-flight (TOF) method,[29–31] AC conductivity,[32,33] microwave conductivity,[34–36] and field-effect mobility measurements.[37–39] In columnar and smectic phases, π-conjugated units aggregate to form one-dimensional columnar stackings or two-dimensional layers in which electronic charges are efficiently transported.[40] The TOF method can reveal macroscopic carrier transport including trapping events in localized states while the microwave conductivity measurement evaluates microscopic band mobilities.[41–43]

Macroscopic carrier transport in ordered columnar phases of a triphenylene dimer and perylene bisimide derivatives were described using a one-dimensional Gaussian disorder model based on charge carrier hopping.[44–47] In ordered smectic phases of terthiophene derivatives, the charge carrier transport process was also

[a] *Program in Advanced Materials Science, Faculty of Engineering and Design, Kagawa University, 2217-20 Hayashi-cho, Takamatsu, Kagawa 761-0396, Japan. E-mail: funahashi.masahiro@kagawa-u.ac.jp*

[b] *Health and Medical Research Institute, National Institute of Advanced Industrial Science and Technology, 2217-14 Hayashi-cho, Takamatsu, Kagawa 761-0395, Japan*

† Electronic supplementary information (ESI) available: Synthetic procedures and spectral data of liquid crystal compounds and synthetic intermediates. Polarizing micrographic textures of liquid crystals. See DOI: https://doi.org/10.1039/d2ma00899h

‡ Present address: Nikon Corporation, Minato-ku, Tokyo 108-6290, Japan.

§ Present address: Sharp Display Company, Kameyama, Mie 519-0198, Japan.
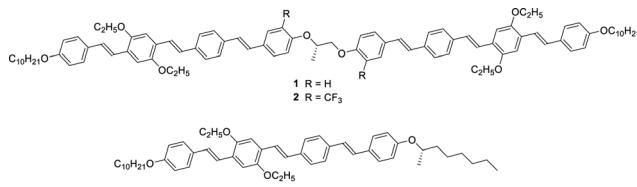
Scheme 1 Molecular structures of N* liquid crystals based on tri(p-phenylene vinylene) units.

Scheme 2 Molecular structures of N* liquid crystals reported previously.

explained using a two-dimensional Gaussian disorder model.[48–50] On the other hand, band-like transport was also reported in a smectic crystal phase and ordered columnar phases.[51–54]

In contrast, N and N* phases have only an orientational order but not a positional order, resulting in low intermolecular π-orbital overlaps. In low molecular weight systems, ionic transport is usually predominant.[55–57] The electronic charge carrier transport has been observed in the N and N* phases of low molecular weight compounds consisting of extended π-conjugated units.[58–62] A few N dyes have been applied in organic thin film solar cells.[63,64] Efficient electronic charge carrier transport has also been confirmed in N conjugated polymers.[65,66] However, the carrier transport mechanism in the N* phase has not been sufficiently studied[67,68] because the number of the organic semiconductors exhibiting the N* phase in a wide temperature range has been limited so far.

N* liquid crystals based on chiral dimeric structures have been designed for glassy film materials for image-recording.[69] We have reported circularly polarized fluorescence with high dissymmetry factors from N* liquid crystals with a dimeric structure.[28,70] Mixtures of oligo(p-phenylene vinylene)-based chiral dimers formed glassy N* films which emitted circularly polarized fluorescence with the dissymmetry factor exceeding 1.4 although the reflection band was not tunable. The carrier transport was studied by the TOF method. The dimeric compound indicated a weak and dispersive transient photocurrent in the N* phase, and the carrier mobilities could not be determined. The LC mixture exhibited hole transport with the mobility on the order of 10^{-4} cm^2 V^{-1} s^{-1} in the N* phase only in a narrow temperature range above 150 °C and the carrier transport mechanism could not be discussed.[70]

In this study, we synthesized chiral dimers **1** and **2** as well as a chiral monomer **3** based on tri(p-phenylene vinylene) units (Scheme 1). These compounds exhibited the N* phase and the mixture of compounds **1–3** exhibited a glassy N* phase at room temperature. The reflection band of the mixture was tunable by the change of the temperature from which the mixture was cooled rapidly. Hole mobilities in the N* phase of compounds **1–3** and the mixture were determined over wide temperature ranges by the TOF method and hole transport characteristics in the N* phase were discussed based on the Gaussian disorder model.

Experimental

Materials

Extended π-conjugated units usually promote crystallization to break helical structures. In order to inhibit the crystallization,
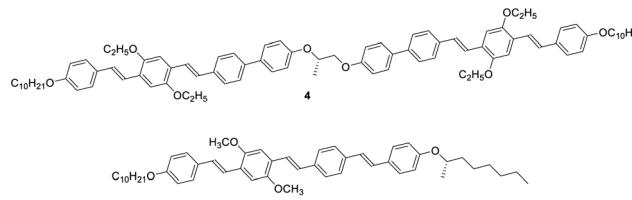
lateral substituents are often necessary. We have previously reported a chiral dimer **4** based on di(p-phenylene vinylene) and biphenyl units as well as monomeric N* liquid crystal **5**, as shown in Scheme 2.[70] In this study, we synthesized compounds **1** and **2** comprising of tri(p-phenylene vinylene) units which have a planar conformation unlike compound **4** including non-planar biphenyl units. Compound **2** has trifluoromethyl groups which inhibit crystallization and stabilize the meso-phase. Compound **3** has ethyl groups at the lateral positions unlike compound **5** bearing methyl groups. The ethyl groups are bulkier than the methyl groups and inhibit crystallization of the π-conjugated units. Compounds **1–3** were synthesized by the synthetic route indicated in Scheme S1 (ESI†). NMR spectra of these compounds are shown in Fig. S1–S3 (ESI†).

Characterization of mesophases

The mesophase structures were characterized by polarizing optical microscopy (POM) and X-ray diffraction. An optical texture of the N* phase was studied using a polarized light microscope equipped with a hand-made hot stage. The phase transition temperature and the transition enthalpy were determined by differential scanning calorimetry (DSC).

Determination of carrier mobility

The carrier mobilities were determined by a time-of-flight (TOF) method under atmospheric conditions.[41–43] A sample in the isotropic phase was capillary-filled into an LC cell consisting of two ITO-coated glass plates on a hot stage. Using a Nd:YAG pulse laser (Continuum MiniLite II), excitation light (wavelength = 356 nm) was illuminated on one side of the cell, with a DC voltage application by an electrometer (ADC R8252). As shown in the birefringent optical textures under observation of a polarizing optical microscope (Fig. S4 and S5, ESI†), the LC molecules aligned parallel to the ITO electrode surfaces in the TOF measurements. The penetration depth of the laser pulse was much shorter than the sample thickness because the chiral nematic compound exhibited a strong absorption band around 400 nm. Therefore, a sheet of photocarriers was generated near the illuminated electrode. The photocarriers sheet drifted across the bulk of the sample under the electric field, inducing a displacement current which was recorded as a voltage drop through a serial resistor using a digital oscilloscope (Tektronics TDS 3044B). The drift of the photogenerated carriers produced a constant photocurrent which decreased to zero when they arrived at the counter electrode. The transit time t_T was determined from the kink points of the transient photocurrent curves. The carrier

mobility μ was calculated from eqn (1), where d is the cell thickness and V is the applied voltage.

$$\mu = \frac{d^2}{V t_T} \qquad (1)$$

Measurement of circularly polarized reflection and photoluminescence spectra of the N* phase

Circularly polarized photoluminescence and reflection spectra were recorded using an Ocean Optics spectrometer (Frame-XR1-ES) equipped with polarizer, and $\lambda/4$ plates and a semiconductor laser with the excitation wavelength of 405 nm or a halogen lamp. The handedness of the CPL luminescence is determined by the order of the two filters. For the optical measurements, the molten liquid crystal samples were capillary-injected into a cell consisting of two glass plates on a hot stage heated over 210 °C. The thickness was controlled by silica particles or polymer films as a spacer. The surfaces of the glass substrates were hydrophilized by UV-O$_3$ treatment and a mechanically rubbed polyimide (PI) alignment layer was prepared on the glass substrate. Butyl cellosolve solutions of PI varnish (SE-150 (0821)) and thinner (26 thinner) supplied from Nissan Chemical Industries were mixed at a ratio of 1:2, respectively. The mixture was spun onto a glass plate at rates of 500 rpm for 10 s, 1500 rpm for 10 s, and 3000 rpm for 20 s. The glass plate was annealed in an oven for 3 hours at 200 °C and the surfaces of the PI thin films deposited on the glass plate were rubbed along the longitudinal direction of the substrates.

Results and discussion

Phase transition properties of compounds 1–3

Polarizing optical micrographs of compounds 1–3 are shown in Fig. S4 (ESI†). DSC thermograms of compounds 1–3 and the mixture of these compounds (molar ratio of 1:2:3 = 4:2:3) are represented in Fig. 1.
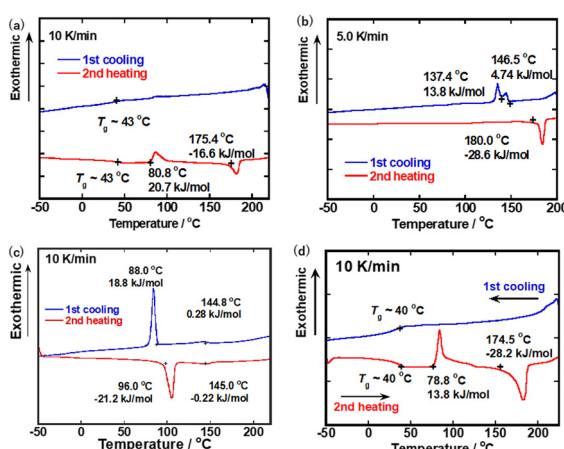

Fig. 1 DSC thermograms in the first cooling and second heating processes for (a) compound 1, (b) 2, (c) 3, and (d) a mixture of compounds 1–3 (molar ratio of 1:2:3 = 4:2:3).

Compound 1 exhibited an N* phase in a cooling process. Below 210 °C, birefringent optical texture with defect lines was observed, which was typical of the N* phase (Fig. S4(a), ESI†). As shown in Fig. 1(a), DSC peaks corresponding to the phase transitions between the isotropic and N* phases were not observed in the heating and cooling processes. This should be attributed to the liquid-like aggregation structure of the N* phase at the phase transition point. On cooling, glass transition was observed around 43 °C. On heating, glass transition occurred around 43 °C. An exothermal peak corresponding to the crystallization of the glassy N* phase appeared at 81 °C and an endothermal peak for melting of the crystal phase to the N* phase was observed at 175 °C. When the sample was cooled rapidly from the N* phase, the N* phase could be retained at room temperature for several hours.

Compound 2 also exhibited a monotropic N* phase in a cooling process. As shown in Fig. S4(b) (ESI†), the homogenous birefringent texture typical of the N* phase was observed when the sample was cooled below 180 °C. As displayed in Fig. 1(b), DSC peaks for the phase transitions between the isotropic and N* phases were not also observed in the heating and cooling processes. On cooling, the N* phase crystallizes at 137 °C via an unidentified mesophase with a narrow temperature range. On heating, an endothermal peak for the transition from the crystal phase to the isotropic phase was observed at 180 °C. Compound 2 also retained the N* phase for several hours at room temperature if the sample was cooled rapidly from the N* phase. The phase transition temperature from the isotropic phase to the N* phase was 30 degrees lowered compared to that of compound 1 because of the bulkiness of the trifluoromethyl groups.

Compound 3 exhibited an enantiotropic N* phase. Fig. S4(c) (ESI†) shows a Grandjan texture in the N* phase of compound 3 at 130 °C. Fig. 1(c) indicates DSC thermograms of compound 3. Unlike dimeric compounds 1 and 2, DSC peaks for the transition between the isotropic and N* phases were recognized at 145 °C in heating and cooling processes. Below 88 °C, compound 3 crystallized and the N* phase could not be retained at room temperature.

Phase transition property of a mixture of compounds 1–3

When compounds 1–3 are cooled gradually, each compound crystallizes at room temperature individually. Consequently, a stable glassy N* film could not be obtained at room temperature. To form more stable glassy N* films, we prepared a mixture of compounds 1–3 with a molar ratio of 4:2:3, respectively. Fig. S5 (ESI†) shows polarizing optical micrographs of the mixture. The Grandjan texture in the N* phase was retained at room temperature. The color difference between these photographs was attributed to the extension of the helical pitch of the sample.

Fig. 1(d) displays DSC thermograms of the mixture. The phase transition peak from the isotropic phase to the N* phase on cooling was ambiguous in compounds 1 and 2. The clearing point on cooling was determined to be 203 °C by POM observation. It is noted that clear glass transition was observed around 40 °C on cooling and heating. In the heating process, the glassy nematic

Table 1 Phase transition temperatures of compounds **1**, **2**, and **3** as well as a mixture of compounds **1**, **2**, and **3** (molar ratio of **1** : **2** : **3** = 4 : 2 : 3)

	Phase transition temperature/°C (cooling/heating)
1	Iso 225[a] N* 43 glassy N*/glassy N* 81 cryst. 175.4 N* 225[a] Iso
2	Iso 180[a] N* 146.5 SmX 137.4 cryst./cryst. 180.0 Iso
3	Iso 144.8 N* 88.0 cryst./cryst. 96.0 N* 145.0 Iso
Mixture	Iso 220[a] N* 40 glassy N*/glassy N* 78.8 cryst. 174.5 Iso

[a] Phase transition temperatures were determined by POM observation.

phase crystallized at 79 °C and the crystal phase melt at 175 °C. In this ternary mixture, a stable glassy N* sample could be produced by dipping the sample in the N* phase into ice water. The glassy N* phase was stable for more than several months at room temperature. The phase transition temperatures of compounds **1–3** and the mixture of compounds **1–3** are summarized in Table 1.

Hole transport in the N* phase of compounds 1–4

Carrier transport characteristics of compounds **1–3** were measured by the TOF method which revealed a macroscopic drift mobility. Fig. 2 shows transient photocurrent curves for holes in the N* phase of compounds **1–4**. It should be noted that non-dispersive transient photocurrents were obtained in the N* phase of compounds **1–3** while a weak dispersive photocurrent response in the N* phase of compound **4**, indicated that the efficient carrier transport did not occur in the N* phase of compound **4**. The hole mobilities in the N* phase of compounds **1–3** were on the order of 10^{-4} cm^2 V^{-1} s^{-1}, which was comparable to those in the N* phase of fluorene- and phenylquaterthiophene-based liquid crystals[62,66,67] and two orders of magnitude higher than ionic mobility in the nematic
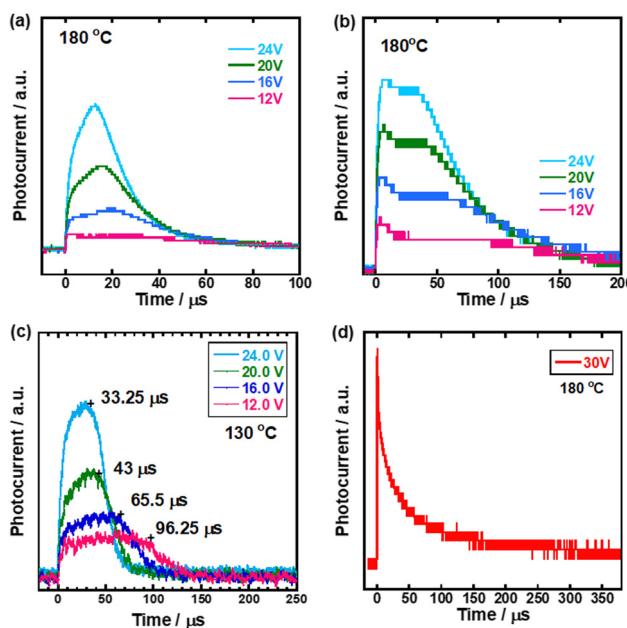
phase of 4-cyano-4′-pentylbiphenyl.[56,57] Compounds **1–3** have planar tri(p-phenylene vinylene) units in contrast to compound **4** of which the π-conjugated unit included a non-planar biphenyl moiety. The planarity of the π-conjugated units of compounds **1–3** should improve the hole transport characteristics in the N* phase. For electrons, only a weak dispersive photocurrent response was obtained and electron mobilities could not be determined by the TOF method.

Fig. 3(a) exhibits Arrhenius plots of the hole mobilities at the electric field of 5×10^4 V cm^{-1} in the N* phase of compounds **1–3** and a mixture of compounds **1–3** (molar ratio of **1** : **2** : **3** = 4 : 2 : 3). Different from smectic and columnar phases in which temperature-independent carrier mobility is often observed,[29,30,35,47] the hole mobilities in the N* phase of these compounds were temperature-dependent.

The hole mobility in the N* phase of compound **3** exceeded 1×10^{-4} cm^2 V^{-1} s^{-1}, indicating an Arrhenius type temperature-dependence with the activation energy of 0.22 eV while the dependence of the hole mobility on the electric field was weak, as shown in Fig. 3(b). The hole mobility was higher than that of a LC chiral dimer based on phenylterthiophene units.[28] The activation energy was comparable to those of monomeric LC quaterthiophene derivatives.[27] This characteristic of the hole mobility in the N* phase of compound **3** should be attributed to the thermally activated hopping of holes, affected by the thermal motion of the LC molecules because the N* phase was fluidic.

Compared to monomeric compound **3**, the N* phase of compounds **1** and **2** was non-fluidic and highly viscous. The hole transport in the N* phase of dimeric compounds **1** and **2** were characterized by the higher activation energy and strong dependence on the temperature. As shown in Fig. 3(a), the activation energies of the hole transport in the N* phase of compounds **1** and **2** were 0.27 eV and 0.37 eV, respectively. These were higher than that in the N* phase of compound **3**.

Fig. 4 represents the hole mobilities plotted for the square root of the electric field in the N* phase of compounds **1** and **2** at various temperatures. The hole mobilities increased with an increase in the electric field and the dependence on the electric field decreased with an increase in the temperature. These characteristics are usually observed in organic amorphous semiconductors such as triphenylamine derivatives and described by the Gaussian disorder model.[71,72] In the Gaussian disorder model, charge carriers transported in the density of states


Fig. 2 Transient photocurrent curves for holes in the N* phase of (a) compound **1** at 180 °C, (b) **2** at 180 °C, (c) **3** at 130 °C, and (d) **4** at 180 °C. The sample thickness was 4 μm and the wavelength of the excitation pulse was 356 nm.
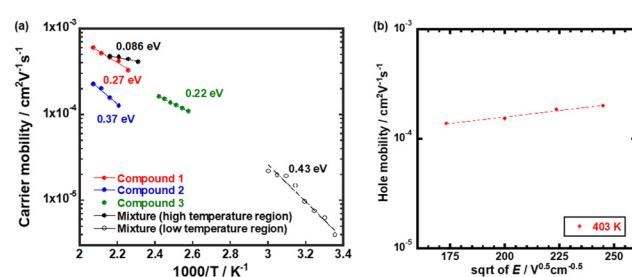

Fig. 3 (a) Arrhenius plots of the hole mobilities in the N* phase of compounds **1–3**. (b) Poole–Frenkel plot of the hole mobility in the N* phase of compound **3**.
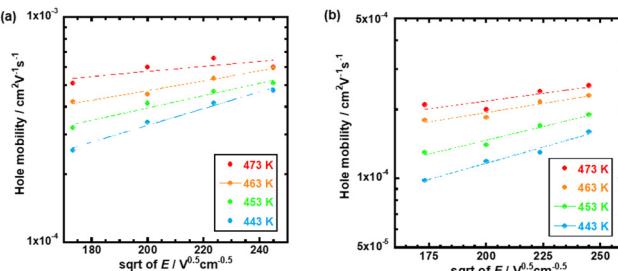
Fig. 4 Hole mobilities plotted for the square root of the electric field at various temperatures in the N* phase of (a) compound **1** and (b) compound **2**.

(DOS) with a Gaussian distribution caused by a disorder of π-orbital energy levels. The carrier transport is characterized by σ, a width of Gaussian DOS, Σ, a disorder of intermolecular orbital overlaps, and μ_{00}, a preexponential factor determined by a transfer integral between π-conjugated units. The carrier mobility μ is described by these parameters in eqn (2) and (3), where T, F, and k_B are temperature, electric field, and the Boltzmann constant, respectively.

$$\mu = \mu_{00} \exp\left[-\left(\frac{2}{3}\frac{\sigma}{k_B T}\right)^2\right]\exp\left[C\left\{\left(\frac{\sigma}{k_B T}\right)^2 - \Sigma^2\right\}\sqrt{F}\right] \quad \text{for } \Sigma \geq 1.5 \tag{2}$$

$$\mu = \mu_{00} \exp\left[-\left(\frac{2}{3}\frac{\sigma}{k_B T}\right)^2\right]\exp\left[C\left\{\left(\frac{\sigma}{k_B T}\right)^2 - 2.25\right\}\sqrt{F}\right] \quad \text{for } \Sigma \leq 1.5 \tag{3}$$

In order to abstract the disorder parameters, zero-field mobility μ_0 was determined at various temperatures by extrapolating μ to $F = 0$ in the plots in Fig. 5. Eqn (4) on μ_0 is derived from eqn (2) and (3), where μ_{00} is a preexponential factor.

$$\mu_0 = \mu_{00}\exp\left[-\left(\frac{2}{3}\frac{\sigma}{k_B T}\right)^2\right] \tag{4}$$

The field-dependence of the hole mobility, β is defined by eqn (5) and can be determined as a slope of a plot at each temperature in Fig. 5.

$$\beta = \frac{\partial \log\mu}{\partial\sqrt{F}} = C\left\{\left(\frac{\sigma}{k_B T}\right)^2 - \Sigma^2\right\} \tag{5}$$

As shown in Fig. 5, μ_{00} was obtained as μ_0 with $1/(k_B T)^2$ of zero and σ was calculated from the slope of the plot of μ_0 for $1/(k_B T)^2$, using eqn (4). The special disorder Σ was determined from the intercept of the plot of β for $1/(k_B T)^2$, based on eqn (5).

In the N* phase of both compounds **1** and **2**, good fits for μ_0 and β to $(1/k_B T)^2$ were obtained, providing disorder parameters as indicated in Table 2. The preexponential factor μ_{00} indicates a virtual mobility without disorders and mainly affected from transfer integral between π-conjugated chromophores of the LC molecules. Compound **1** exhibits a high μ_{00} value on the order
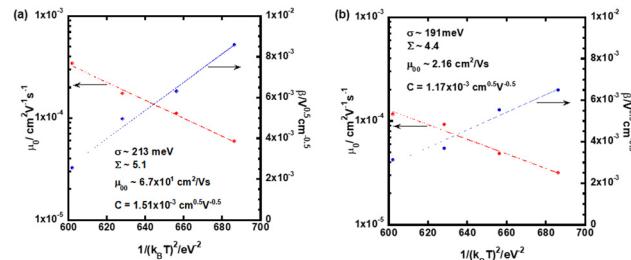

Fig. 5 Plots of zero-field mobility μ_0 and field-dependence of the hole mobility β as a function of the square of $1/k_B T$ in the N* phase of (a) compound **1** and (b) compound **2**.

Table 2 Disorder parameters in the N* phase of compounds **1** and **2**

Compound	$\mu_{00}/\text{cm}^2\ \text{V}^{-1}\ \text{s}^{-1}$	σ/meV	Σ	$C/\text{cm}^{0.5}\ \text{V}^{0.5}$
1	6.7×10^1	213	5.1	1.5×10^{-3}
2	2.2	191	4.4	1.2×10^{-3}

of 10 cm^2 V^{-1} s^{-1}, which is one order of magnitude higher than that of compound **2**. This value is also higher than those of organic amorphous semiconductors of which μ_{00} is typically 0.01–1 cm^2 V^{-1} s^{-1}.[73–75] This should be attributed to the extended planar tri(p-phenylene vinylene) unit of compound **1**, which can stack closely in the N* phase. Compared to compound **1**, trifluoromethyl groups of compound **2** should inhibit close aggregation of the π-conjugated units in the N* phase, resulting in a smaller μ_{00} value than that of compound **1**.

Energetic and spatial disorders, σ and Σ of compound **2** were smaller than those of compound **1**, indicating a more ordered structure in the N* phase of compound **2** compared to the N* phase of compound **1**. Steric hindrance originated from the bulky trifluoromethyl groups of compound **2** weakened intermolecular interaction between the π-conjugated units to increase the mobility of the chromophores, resulting in the decrease of disorders in the N* phase of compound **2**.

Hole transport in the N* phase of the mixture of compounds 1–3

Preparation of mixtures of the N* liquid crystals is required for tuning of the reflection band in the CPL emission and formation of more stable glassy N* states. Carrier transport properties in the N* phase of the mixture of compounds **1–3** (molar ratio of **1**:**2**:**3** = 4:2:3) were also studied by the TOF method. In the DSC measurements, the mixture formed a glassy N* phase at a cooling rate of 10 K min^{-1}. When the mixture was cooled more slowly, it could retain the N* phase on cooling from 190 °C to 150 °C. However, the mixture gradually crystallized around 140 °C. The mixture formed a glassy N* phase when it was cooled from the N* phase around 180 °C by being dipped in water. The glassy N* phase was retained up to 65 °C and gradually crystallized when it was heated above 70 °C. Precisely, the phase between 40 °C (glass transition temperature determined in the DSC measurement) and 65 °C should be the supercooled N* phase.

Therefore, the TOF measurement was carried out in the temperature ranges of the N* phase in which the sample was cooled from 200 °C to 160 °C and of the supercooled N* phase
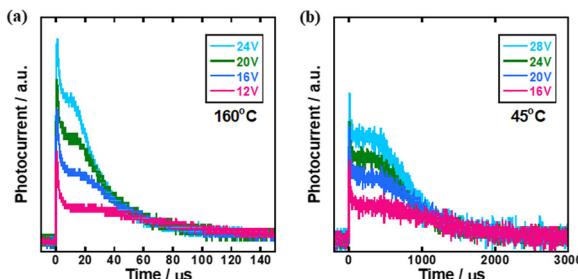
Fig. 6   Transient photocurrent curves for holes (a) in the N* phase of the mixture of compounds **1–3** at 160 °C and (b) in the glassy N* phase at 45 °C. The sample thickness was 4 μm and the wavelength of excitation light was 356 nm.

in which the sample was heated from 25 °C to 60 °C. Fig. 6 shows transient photocurrent curves for holes in the N* phase in the high and low temperature regions of the mixture of compounds **1–3**. In both temperature regions, non-dispersive transient photocurrent responses were obtained and hole mobilities could be determined although the photocurrent response was so low that the transit time could not be determined below room temperature.

Fig. 7(a) displays the hole mobility as a function of square root of the electric field in the high temperature region of the N* phase of the mixture. In this region, the temperature- and field-dependence of the hole mobility was not so remarkable compared to those in the N* phase of compounds **1–3**, as shown in Fig. 7. The activation energy in the high temperature region was 0.086 eV as indicated in Fig. 3(a). As exhibited in Fig. 7(b), the fitting of the plots provided μ_{00}, σ, and Σ to be 7.7×10^{-4} cm^2 V^{-1} s^{-1}, 63 meV, and 0.99, respectively. However, the experimental errors should be very large. Compared to the N* phase of compounds **1** and **2**, the viscosity of the mixture was lower and indicated fluidity. The charge carrier hopping process in the high temperature region of the N* phase of the mixture should be affected by molecular dynamic motion. The Gaussian disorder model based on a static solid lattice should not be valid for the high temperature N* phase with the dynamic nature. In the columnar and smectic phases, the Gaussian disorder model described the carrier transport characteristics well below room temperature although it could
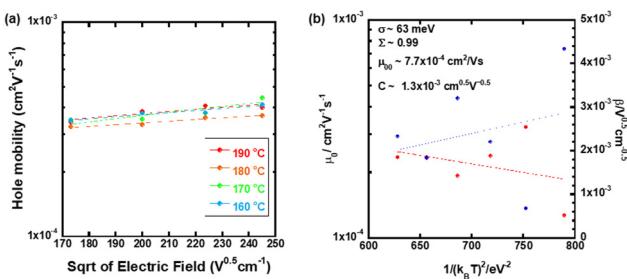
not be applied to these phases above room temperature, where the mobilities were independent of the temperature and electric field. In some cases, the carrier mobilities indicated negative temperature-dependence.[47,50]

The N* phase should be a glassy N* phase below 40 °C and should be a super cooled N* phase between 45 °C and 65 °C. In these N* phases, the viscosities were sufficiently low and could be regarded as solids to which the Gaussian disorder model could be applied.

Fig. 8(a) shows the hole mobility as a function of the square root of the electric field in the low temperature region of the N* phase of the mixture. Compared to the N* phase of compounds **1** and **2**, the field-dependence of the hole mobility was not remarkable while the hole mobility depended upon the temperature strongly. The activation energy of the hole mobility was 0.43 eV assuming the Arrhenius-type temperature-dependence, as shown in Fig. 3(a). The temperature-dependence of the hole mobility decreased with an increase in the temperature, and it changed to be negative above 318 K. This behavior was similar to that of organic amorphous solids to which the Gaussian disorder model can be applied.

Fig. 8(b) represents the plots of zero-field mobility μ_0 and β for the $1/(k_B T)^2$. They revealed the disorder parameters, μ_{00}, σ, and Σ to be 6.0 cm^2 V^{-1} s^{-1}, 149 meV, and 5.3, respectively. The preexponential parameter μ_{00} was larger than that in the N* phase of compound **2**, but lower than that in the N* phase of compound **1**. In the mixture, the intermolecular π-orbital overlaps should be averaged between those of compounds **1** and **2**. Energetic and spatial disorders σ and Σ were lower than those of compounds **1** and **2**. This should be attributed to the effective immobilization of the N* structure with low disorders in the high temperature region of the N* phase of the mixture into the glassy and supercooled N* phases of the mixture by the rapid cooling.

The hole transport in the N* phase of these tri(p-phenylene vinylene)-based liquid crystals was characterized by large μ_{00} as well as large energetic and special disorders. In amorphous organic solids such as triphenylamine derivatives, μ_{00} values are typically 10^{-2}–10^{-1} cm^2 V^{-1} s^{-1}.[75] In the N* phase of compounds **1** and **2** as well as the mixture of compounds **1–3**,


Fig. 7   (a) Hole mobilities plotted for the square root of the electric field at various temperatures in the N* phase of the compounds **1–3** mixture (high temperature region). (b) Plots of zero-field mobility μ_0 and β as a function of the square of $1/k_B T$ in the N* phase of the LC mixture (high temperature region).
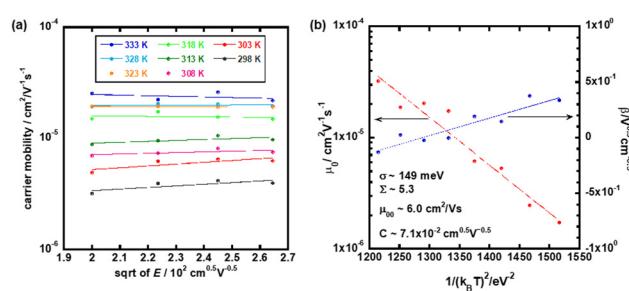
Fig. 8   (a) Hole mobilities plotted for the square root of the electric field at various temperatures in the N* phase of the compounds **1–3** mixture (low temperature region). (b) Plots of zero-field mobility μ_0 and β as a function of the square of $1/k_B T$ in the N* phase of the LC mixture (low temperature region).

the planar extended tri(p-phenylene vinylene) units aggregated effectively to increase the intermolecular hole transfer rate in contrast to non-planar triphenylamine derivatives.

The disorder parameters σ and Σ are typically 100 meV and 2 in organic amorphous solids based on triphenylamine units.[75] The characteristic feature of compounds **1–3** is the extended π-conjugated unit with a large aspect ratio. The disorder parameters σ and Σ in the N* phase of these compounds were larger than those in the organic amorphous solids although the LC molecules locally oriented uniaxially in the N* phase. The energetic disorder σ is affected by local electric fields produced by electrical dipoles of molecules. The π-conjugated unit of compounds **1–3** with a large aspect ratio exhibit a higher polarizability, resulting in larger energetic disorder compared to the isotropic extended π-orbitals of triphenylamine-based organic amorphous solids. The larger spatial disorder Σ in the N* phase should also be attributed to the anisotropic molecular shape of compounds **1–3**.

In the N* phase, the LC molecules locally orient uniaxially and form a helical structure macroscopically while π-conjugated units stack within layers or columns in the smectic or columnar phases, respectively. In spite of the absence of π–π stacking structures in the N* phase, the preexponential parameters (μ_{00}) in the N* phase of compounds **1** and **2** as well as the mixture of compounds **1–3** were comparable to those in the columnar and smectic phases.[44–50] This should be attributed to the extended and planar π-conjugated units in compounds **1–3**. The energetic and spatial disorders σ and Σ are around 50 meV and 1.5–2 in the smectic and columnar phases. Those parameters in the N* phase of compounds **1** and **2** as well as the mixture were much larger than those in the smectic and columnar phases.[44–50] This should be attributed to the more disordered structure in the N* phase than those in the smectic and columnar phases.

O'Neill and coworkers studied hole transport characteristics in the nematic phase of a cross-linked LC semiconductor based on correlated disorder model. In the N phase, the energetic and spatial disorders were 89 meV and 2.4, respectively.[67] Compared to these values, the energetic and spatial disorders in the N* phase of compounds **1** and **2** as well as the mixture were much larger. The tri(p-phenylene vinylene) units are connected by a chiral moiety and the conformation of the π-conjugated units was restricted in these compounds. This conformation restriction should inhibit local uniaxial alignment of the π-conjugated units to increase the energetic and spatial disorders.

Tuning of the reflection band and CPL emission from the mixture

Compounds **1–3** could not form a stable glassy N* film independently. Moreover, the reflection bands of compounds **1** and **2** were positioned in the ultraviolet region while that of compound **3** was in the infrared area. In order to obtain the CPL emission from the N* films over a wide wavelength region, the reflection band should be tuned to cover the emission spectrum.

In the mixture of compounds **1–3** (molar ratio of **1** : **2** : **3** = 4 : 2 : 3), the reflection band could be immobilized in the glassy
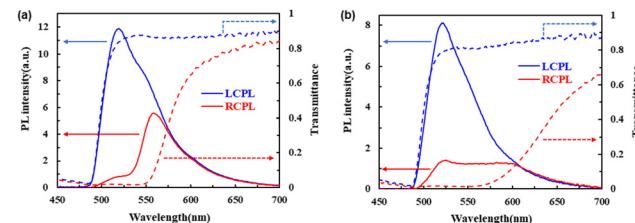

Fig. 9 Photoluminescence and transmittance spectra at room temperature from the glassy N* film of the mixture of compounds **1–3** (molar ratio of **1** : **2** : **3** = 4 : 2 : 3), cooled from (a) 220 °C and (b) 175 °C. Blue and red lines are for left- and right-handed circularly polarized fluorescence, respectively. Solid and dashed lines are for fluorescence and reflection spectrum, respectively.

N* phase at room temperature and tuned from the blue to red region by changing the temperature from which the sample was cooled rapidly. Fig. 9 shows fluorescence and transmittance spectra from the glassy N* phase of the mixture at room temperature. When the sample in the N* phase at 220 °C was dipped in ice water, the reflection band edge was immobilized at 580 nm. Below 550 nm, right-handed circularly polarized fluorescence was suppressed while left-handed circularly polarized fluorescence was not affected by the reflection band. When the sample was cooled from 175 °C, the reflection band edge was extended to 630 nm, covering the main part of the emission band. Within the reflection band, right-handed circularly polarized fluorescence was suppressed, providing CPL emission with a dissymmetry factor exceeding 1.4.

The high dissymmetry factor indicates low structural disorder of the N* phase of the mixture. The periodical helical structure of the N* phase should not be perturbed by mixing the three compounds. The low disorder parameters σ and Σ determined by the TOF measurement in the N* phase of the mixture should reflect the low structural disorder.

Conclusions

Chiral dimeric N* liquid crystals **1** and **2** as well as monomeric N* liquid crystal **3** based on tri(p-phenylene vinylene) units were synthesized. These dimeric compounds exhibited a monotropic chiral nematic (N*) phase while monomeric compound **3** showed an enantiotropic N* phase. The mixture of compounds **1–3** exhibited a glassy N* phase at room temperature and the reflection band could be tuned by the change of the temperature from which the rapid cooling of the mixture started. When the reflection band covered the fluorescence peak, high quality circularly polarized emission with a dissymmetry factor of 1.4 was observed. Hole mobilities were determined over wide temperature ranges by the TOF method and hole transport characteristics in the N* phase were analyzed using the Gaussian disorder model. The preexponential factors μ_{00}'s in the N* phase of these compounds were on the order of 1 cm^2 V^{-1} s^{-1} which were one or two order of magnitudes higher than those of amorphous organic semiconductors. This should be attributed to the large π-conjugated units of these compounds. The energetic and spatial disorders

exceeded 100 meV and 4, respectively. These values were larger than those of amorphous organic semiconductors in spite of the local uniaxial molecular orientation in the N* phase. This result should originate from the large anisotropic polarizability of the π-conjugated units with a large aspect ratio.

Author contributions

K. M. and E. S. synthesized liquid crystal materials. K. M. also conducted characterization of mesomorphic properties and carrier transport of the liquid crystals. S. M. and N. T. measured circularly polarized photoluminescence of the liquid crystal compounds. M. F. conducted analysis of carrier transport characteristics in the N* phase and planned this study.

Conflicts of interest

There are no conflicts to declare.

Acknowledgements

Notes and references

1 M. O'Neill and S. M. Kelly, Ordered materials for organic electronics and photonics, *Adv. Mater.*, 2010, **23**, 566–584.

2 M. Funahashi, Nanostructured liquid-crystalline semiconductors – a new approach to soft matter electronics, *J. Mater. Chem. C*, 2014, **2**, 7451–7459.

3 T. Kato, M. Yoshio, T. Ichikawa, B. Soberats, H. Ohno and M. Funahashi, Transport of ions and electrons in nanostructured liquid crystals, *Nat. Rev. Mater.*, 2017, **2**, 17001.

4 M. Funahashi, Solution-processable electronic and redox-active liquid crystals based on the design of side chains, *Flexible Printed Electron.*, 2020, **5**, 043001.

5 T. Hassheider, S. A. Benning, H.-S. Kitzerow, M.-F. Achard and H. Bock, Color-tuned electroluminescence from columnar liquid crystalline alkyl arenecarboxylates, *Angew. Chem., Int. Ed.*, 2001, **40**, 2060–2063.

6 M. P. Aldred, A. E. A. Contoret, S. R. Farrar, S. M. Kelly, D. Mathieson, M. O'Neill, W. C. Tsoi and P. Vlachos, A full color electroluminescence device and patterned photoalignment using light emitting liquid crystal, *Adv. Mater.*, 2005, **17**, 1368–1372.

7 Y. Wang, J. Shi, J. Chen, W. Zhu and E. Baranoff, Recent progress in luminescent liquid crystal materials: Design, properties and application for linearly polarised emission, *J. Mater. Chem. C*, 2015, **3**, 7993–8005.

8 M. Funahashi, Development of liquid crystalline semiconductors with high carrier mobility and their application to thin-film transistors, *Polym. J.*, 2009, **41**, 459–469.

9 W. Pisula, A. Menon, M. Stepputat, I. Lieberwirth, U. Kolb, A. Tracz, H. Sirringhaus, T. Pakula and K. Müllen, A zone casting technique for device fabrication of field-effect transistors based on discotic hexa-*peri*-hexabenzocoronene, *Adv. Mater.*, 2005, **17**, 684–689.

10 A. J. J. M. van Breemen, P. T. Herwig, C. H. T. Chlon, J. Sweelssen, H. F. M. Schoo, S. Setayesh, W. M. Hardeman, C. A. Martin, D. M. de Leeuw, J. J. P. Valeton, C. W. M. Bastiaansen, D. J. Broer, A. R. Popa-Merticaru and S. C. J. Meskers, Large area liquid crystal Monodomain field-effect transistors, *J. Am. Chem. Soc.*, 2006, **128**, 2336–2345.

11 M. Funahashi, F. Zhang and N. Tamaoki, High ambipolar mobility in highly ordered smectic phase of dialkylphenylterthiophene derivative that can be applied to solution-processed organic field effect transistors, *Adv. Mater.*, 2007, **19**, 353–358.

12 H. Iino, T. Usui and J. Hanna, Liquid crystals for organic thin-film transistors, *Nat. Commun.*, 2015, **6**, 6828.

13 L. Schmidt-Mende, A. Fechtenkötter, K. Müllen, E. Moons, R. H. Friend and J. D. MacKenzie, Self-organized discotic liquid crystals for high-efficiency organic photovoltaics, *Science*, 2001, **293**, 1119–1122.

14 T. Hori, Y. Miyake, N. Yamasaki, H. Yoshida, A. Fujii, Y. Shimizu and M. Ozaki, Solution processable organic solar cell based on bulk heterojunction utilizing phthalocyanine derivative, *Appl. Phys. Express*, 2010, **3**, 101602.

15 K. Sun, Z. Xiao, S. Lu, W. Zajaczkowski, W. Pisula, E. Hanssen, J. M. White, R. M. Williamson, J. Subbiah, J. Ouyang, A. B. Holmes, W. W. H. Wong and D. J. Jones, A molecular nematic liquid crystalline material for high-performance organic photovoltaics, *Nat. Commun.*, 2015, **6**, 6013.

16 M. Funahashi, Anisotropic electrical conductivity of n-doped thin films of polymerizable liquid-crystalline perylene bisimide bearing a triethylene oxide chain and cyclotetrasiloxane rings, *Mater. Chem. Front.*, 2017, **1**, 1137–1146.

17 T. Taga, S. Takaoka, S. Uemura and M. Funahashi, Liquid-crystalline perylene bisimide derivatives bearing an aza-crown ether ring complexing with alkaline metal ions, *Mater. Chem. Front.*, 2022, **6**, 880–890.

18 Y. Funatsu, A. Sonoda and M. Funahashi, Ferroelectric liquid-crystalline semiconductors based on a phenylterthiophene skeleton: Effect of introduction of oligosiloxane

moieties and photovoltaic effect, *J. Mater. Chem. C*, 2015, **3**, 1982–1993.

19 A. Seki, Y. Funatsu and M. Funahashi, Anomalous photovoltaic effect based on molecular chirality: Influence of enantiomeric purity on the photocurrent response in π-conjugated ferroelectric liquid crystals, *Phys. Chem. Chem. Phys.*, 2017, **19**, 16446–16455.

20 M. Funahashi, High open-circuit voltage in the bulk photovoltaic effect for the chiral smectic crystal phase of a double chiral ferroelectric liquid crystal doped with a fullerene derivative, *Mater. Chem. Front.*, 2021, **5**, 8265–8274.

21 M. Funahashi and Y. Mori, Linearly polarized electroluminescence device in which the polarized plane can be rotated electrically using a chiral liquid crystalline semiconductor, *Mater. Chem. Front.*, 2020, **4**, 2137–2148.

22 S. H. Chen, D. Katsis, A. W. Schmid, J. C. Mastrangelo, T. Tsutsui and T. N. Blanton, Circularly polarized light generated by photoexcitation of luminophores in glassy liquid-crystal films, *Nature*, 1999, **397**, 506–508.

23 H. Finkelmann, S. T. Kim, A. Munoz, P. Palffy-Muhoray and B. Taheri, Tunable mirrorless lasing in cholesteric liquid crystal-line elastomers, *Adv. Mater.*, 2001, **13**, 1069–1072.

24 M. Funahashi, Chiral liquid crystalline electronic systems, *Symmetry*, 2021, **13**, 672.

25 K. L. Woon, M. O'Neill, G. J. Richards, M. P. Aldred, S. M. Kelly and A. M. Fox, Highly circularly polarized photoluminescence over a broad spectral range from a calamitic, hole-transporting, and chiral nematic glass and from an indirectly excited dye, *Adv. Mater.*, 2003, **15**, 1555–1558.

26 K. L. Woon, M. P. Aldred, P. Vlachos, G. H. Mehl, T. Stirner, S. M. Kelly and M. O'Neill, Electronic charge transport in extended nematic liquid crystals, *Chem. Mater.*, 2006, **18**, 2311–2317.

27 M. Funahashi and N. Tamaoki, Effect of pretransitional organization in cholesteric phases of oligothiophene derivatives on their carrier transport characteristics, *Chem. Mater.*, 2007, **19**, 608–617.

28 T. Hamamoto and M. Funahashi, Circularly polarized light emission from a chiral nematic phenylterthiophene dimer exhibiting ambipolar carrier transport, *J. Mater. Chem. C*, 2015, **3**, 6891–6900.

29 D. Adam, F. Closs, T. Frey, D. Funhoff, D. Haarer, P. Schuhmacher and K. Siemensmeyer, Transient photoconductivity in a discotic liquid crystal, *Phys. Rev. Lett.*, 1993, **70**, 457–460.

30 M. Funahashi and J. Hanna, Fast ambipolar carrier transport in smectic phases of phenylnaphthalene liquid crystal, *Appl. Phys. Lett.*, 1997, **71**, 602–604.

31 Y. Miyake, Y. Shiraiwa, K. Okada, H. Monobe, T. Hori, N. Yamasaki, H. Yoshida, M. J. Cook, A. Fujii, M. Ozaki and Y. Shimizu, High carrier mobility up to 1.4 cm^2 V^{-1} s^{-1} in non-peripheral octahexyl phthalocyanine, *Appl. Phys. Express*, 2011, **4**, 021604.

32 N. Boden, R. C. Borner, R. J. Bushby and J. Clements, First Observation of a n-doped quasi-one-dimensional electronically-conducting discotic liquid crystal, *J. Am. Chem. Soc.*, 1994, **116**, 10807–10808.

33 N. Boden, R. J. Bushby and J. Clements, Mechanism of quasi-one-dimensional electronic conductivity in discotic liquid crystals, *J. Chem. Phys.*, 1993, **98**, 5920–5931.

34 A. M. van de Craats, J. M. Warman, A. Fechtenkötter, J. B. Brand, M. A. Harbison and K. Müllen, Record charge carrier mobility in a room-temperature discotic liquid-crystalline derivative of hexabenzocoronene, *Adv. Mater.*, 1999, **11**, 1469–1472.

35 J. Simmerer, B. Gliisen, W. Paulus, A. Kettner, P. Schuhmacher, D. Adam, K.-H. Etzbach, K. Siemensmeyer, J. H. Wendorff, H. Ringsdorf and D. Haarer, Transient photoconductivity in a discotic hexagonal plastic crystal, *Adv. Mater.*, 1996, **8**, 815–819.

36 T. Sakurai, K. Shi, H. Sato, K. Tashiro, A. Osuka, A. Saeki, S. Seki, S. Tagawa, S. Sasaki, H. Masunaga, K. Osaka, M. Takata and T. Aida, Prominent electron transport property observed for triply fused metalloporphyrin dimer: Directed columnar liquid crystalline assembly by amphiphilic molecular design, *J. Am. Chem. Soc.*, 2008, **130**, 13812–13813.

37 F. Zhang, M. Funahashi and N. Tamaoki, High-performance thin film transistors from semiconducting liquid crystalline phases by solution processes, *Appl. Phys. Lett.*, 2007, **91**, 063515.

38 K. Nakano, H. Iino, T. Usui and J.-I. Hanna, Bulk mobility of polycrystalline thin films of quaterthiophene derivatives, *Appl. Phys. Lett.*, 2011, **98**, 103302.

39 S. Cherian, C. Donley, D. Mathine, L. LaRussa, W. Xia and N. Armstrong, Effects of field dependent mobility and contact barriers on liquid crystalline phthalocyanine organic transistors, *J. Appl. Phys.*, 2004, **96**, 5638–5643.

40 W. Pisula, M. Zorn, J. Chang, K. Müllen and R. Zentel, Liquid crystalline ordering and charge transport in semiconducting materials, *Macrmol. Rapid Commun.*, 2009, **30**, 1179–1202.

41 W. E. Spear, Drift mobility techniques for the study of electrical transport properties in insulating solids, *J. Non-Cryst. Solids*, 1968, **1**, 197–214.

42 A. Köhler and H. Bässler, *Electronic Processes in Organic Semiconductors*, Wiley-VCH Verlag GmbH & KGaA, Weinheim, 2015.

43 M. Funahashi, *Time-of-flight method for determining the drift mobility in organic semiconductors, Organic Semiconductors for Optoelectronics*, ed. H. Naito, Wiley interscience, 2021.

44 I. Bleyl, C. Erdelen, H.-W. Schmidt and D. Haarer, One-dimensional hopping transport in a columnar discotic liquid-crystalline glass, *Philos. Mag. B*, 1999, **79**, 463–475.

45 H. Iino, J. Hanna, R. J. Bushby, B. Movaghar and B. J. Whitaker, Hopping conduction in the columnar liquid crystal phase of a dipolar discogen, *J. Appl. Phys.*, 2006, **100**, 043716.

46 L.-Y. Chen, F.-H. Chien, Y.-W. Liu, W. Zheng, C.-Y. Chiang, C.-Y. Hwang, C.-W. Ong, Y.-K. Lan and H. C. Yang, Ambipolar carrier transport properties in a built-in donor–acceptor discogen, *Org. Electron.*, 2013, **14**, 2065–2070.

47 M. Funahashi and A. Sonoda, Electron transport characteristics in nano-segregated columnar phases of perylene tetracarboxylic bisimide derivatives bearing oligosiloxane chains, *Phys. Chem. Chem. Phys.*, 2014, **16**, 7754–7763.

48 A. Ohno and J. Hanna, Simulated carrier transport in smectic mesophase and its comparison with experimental result, *Appl. Phys. Lett.*, 2003, **82**, 751–753.

49 M. Funahashi and J. Hanna, Mesomorphic behaviors and charge transport in terthiophene derivatives, *Mol. Cryst. Liq. Cryst.*, 2004, **410**, 529–540.

50 M. Funahashi, F. Zhang, N. Tamaoki and J. Hanna, Ambipolar transport in the highly ordered smectic phase of 2-alkyl-5″-alkynyl- terthiophene derivative in a wide temperature range, *ChemPhysChem*, 2008, **9**, 1465–1473.

51 M. Funahashi, T. Ishii and A. Sonoda, Temperature-independent hole mobility of a smectic liquid-crystalline semiconductor based on band-like conduction, *ChemPhysChem*, 2013, **14**, 2750–2758.

52 X. Feng, V. Marcon, W. Pisula, M. R. Hanzen, J. Kirkpatrick, F. Grozema, D. Andrienko, K. Kremer and K. Müllen, Towards high charge-carrier mobilities by rational design of the shape and periphery of discotics, *Nat. Mater.*, 2009, **8**, 421–426.

53 W. Pisula, M. Kastler, D. Wasserfallen, M. Mondeshki, J. Piris, I. Schnell and K. Müllen, Relation between supramolecular order and charge carrier mobility of branched alkyl hexa-*peri*-hexabenzocoronenes, *Chem. Mater.*, 2006, **18**, 3634–3640.

54 W. Pisula, X. Feng and K. Müllen, Tuning the columnar organization of discotic polycyclic aromatic hydrocarbons, *Adv. Mater.*, 2010, **22**, 3634–3639.

55 Y. Shimizu, K. Shigeta and S. Kusabayashi, Mesomorphic and photoconducting behavior of 2-(2-hydroxy-4-alkoxybenzyl-ideneamino)-9-methylcarbazoles, *Mol. Cryst. Liq. Cryst.*, 1986, **140**, 105–117.

56 H. Naito, K. Yoshida and M. Okuda, Transient charging current in nematic liquid crystals, *J. Appl. Phys.*, 1993, **73**, 1119–1125.

57 A. Sugimura, N. Matsui, Y. Takahashi, H. Sonomura, H. Naito and M. Okuda, Transient currents in nematic liquid crystals, *Phys. Rev. B: Condens. Matter Mater. Phys.*, 1991, **43**, 8272–8276.

58 M. Funahashi and N. Tamaoki, Electronic conduction in the chiral nematic phase of the oligothiophene derivative, *ChemPhysChem*, 2006, **7**, 1193–1197.

59 K. L. Woon, M. P. Aldred, P. Vlachos, G. H. Mehl, T. Stirner, S. M. Kelly and M. O'Neill, Electronic charge transport in extended nematic liquid crystals, *Chem. Mater.*, 2006, **18**, 2311–2317.

60 M. Funahashi and N. Tamaoki, Effect of pretransitional organization in cholesteric phases of oligothiophene derivatives on their carrier transport characteristics, *Chem. Mater.*, 2007, **19**, 608–617.

61 K. Tokunaga, Y. Takayashiki, H. Iino and J.-I. Hanna, Electronic conduction in nematic phase of small molecules, *Phys. Rev. B: Condens. Matter Mater. Phys.*, 2009, **79**, 033201.

62 M. Nuita, J. Sakuda, Y. Hirai, M. Funahashi and T. Kato, Hole transport of a liquid-crystalline phenylterthiophene derivative exhibiting the nematic phase at ambient temperature, *Chem. Lett.*, 2011, **40**, 412–413.

63 K. Sun, Z. Xiao, S. Lu, W. Zajaczkowski, W. Pisula, E. Hanssen, J. M. White, R. M. Williamson, J. Subbiah, J. Ouyang, A. B. Holmes, W. W. H. Wong and D. J. Jones, A molecular nematic liquid crystalline material for high-performance organic photovoltaics, *Nat. Commun.*, 2015, **6**, 6013.

64 M. Zhang, F. Zhang, Q. An, Q. Sun, W. Wang, X. Ma, J. Zhang and W. Tang, Nematic liquid crystal materials as a morphology regulator for ternary small molecule solar cells with power conversion efficiency exceeding 10%, *J. Mater. Chem. A*, 2017, **5**, 3589–3598.

65 M. Redecker and D. D. C. Bradley, Mobility enhancement through homogeneous nematic alignment of a liquid-crystalline polyfluorene, *Appl. Phys. Lett.*, 1999, **74**, 1400–1402.

66 H. Sirringhaus, R. J. Wilson and R. H. Friend, Mobility enhancement in conjugated polymer field-effect transistors through chain alignment in a liquid-crystalline phase, *Appl. Phys. Lett.*, 2000, **77**, 406–408.

67 S. R. Farrar, A. E. A. Contoret, M. O'Neill, J. E. Nicholls, G. J. Richards and S. M. Kelly, Nondispersive hole transport of liquid crystalline glasses and a cross-linked network for organic electroluminescence, *Phys. Rev. B: Condens. Matter Mater. Phys.*, 2002, **66**, 125107.

68 M. Goto, H. Takezoe and K. Ishikawa, Carrier transport simulation of anomalous temperature dependence in nematic liquid crystals, *Phys. Rev. E: Stat., Nonlinear, Soft Matter Phys.*, 2007, **76**, 040701(R).

69 V. A. Mallia and N. Tamaoki, Design of chiral dimesogens containing cholesteryl groups; formation of new molecular organizations and their application to molecular photonics, *Chem. Soc. Rev.*, 2004, **33**, 76–84.

70 E. Shimaoka, M. Kunihiro and M. Funahashi, Glass-forming chiral liquid crystalline dimers based on oligo(phenylene-vinylene) unit exhibiting circularly polarized photoluminescence, *ACS Appl. Polym. Mater.*, 2022, **4**, 565–574.

71 H. Bässler, Charge transport in disordered organic photo-conductors, A Monte Carlo simulation study, *Phys. Status Solidi B*, 1993, **175**, 15–56.

72 M. van der Auweraer, F. C. de Schryver, P. M. Borsenberger and H. Bässler, Disorder in charge transport in doped polymers, *Adv. Mater.*, 1994, **6**, 199–213.

73 P. M. Borsenberger, L. Pautmeier and H. Bässler, Charge transport in disordered molecular solids, *J. Chem. Phys.*, 1991, **94**, 5447–5454.

74 P. M. Borsenberger, L. Pautmeier and H. Bässler, Hole transport in bis(4-*N,N*-diethylamino-2-methylphenyl)-4-methylphenyl-methane, *J. Chem. Phys.*, 1991, **95**, 1258–1265.

75 Y. Shirota and H. Kageyama, Charge carrier transporting molecular materials and their applications in devices, *Chem. Rev.*, 2007, **107**, 953–1010.